Spatial and temporal complexity of the Amazon flood measured from space

Doug Alsdorf,[1] Paul Bates,[2] John Melack,[3] Matt Wilson,[4] and Thomas Dunne[3]

Received 23 January 2007; revised 26 February 2007; accepted 22 March 2007; published 19 April 2007.

[1] Floodplain processes are driven by water flows that seasonally change in direction and consist of a myriad of interacting streams of varying depth, velocity, source, sediment concentration and chemistry. Here we show, using spaceborne interferometric synthetic aperture radar (SAR) JERS-1 measurements, the first spatially dense hydraulic mapping of the passage of a flood wave through a large, topographically complex floodplain. We find that temporal changes in flood water heights ($\partial h/\partial t$) are more complex than typically assumed. During the passage of a flood wave, sharp variations in $\partial h/\partial t$ are localized along some floodplain channels. These channels separate adjacent locations with different rates of infilling. Near the peak of the flood wave, some of the channels are no longer evident as controls on $\partial h/\partial t$. During the passage of the flood wave, flow paths change from bathymetrically influenced to hydraulically controlled (and back again), thus it is difficult to know the flow path *a-priori* from bathymetry alone. **Citation:** Alsdorf, D., P. Bates, J. Melack, M. Wilson, and T. Dunne (2007), Spatial and temporal complexity of the Amazon flood measured from space, *Geophys. Res. Lett.*, *34*, L08402, doi:10.1029/2007GL029447.

1. Introduction

[2] Recent high-resolution studies of the topography, hydraulics, sedimentology, and ecology of large, natural floodplains have revealed considerable complexity of form and function (e.g., Figure 1). These studies are necessary for understanding how floodplain geomorphology responds to changes of discharge and sediment load [*Dunne et al.*, 1998] and wetland ecosystems respond to inundation and nutrient exchanges [*Melack and Forsberg*, 2001]. For example, *Dunne et al.* [1998] showed that more than 25% of the suspended sediment dispersed into the floodplain from the Amazon River was transported through channels of various sizes, and that the proportion dispersed by diffuse flow varied in time and space. These spatially and temporally fluctuating flows are driven by temporal and spatial gradients of water-surface elevation, floodplain topography, and hydraulic roughness.

[3] Discharge in rivers is measured at channel cross sections with simple geometry producing a one-dimensional measurement. Floodplain and wetland flows are much more complex with both large-scale diffusive and locally confined hydraulics. Because in-situ methods of measuring water surface elevation are made at cross sections it is impractical to measure the extent and elevation of floodwaters over an entire floodplain, and to measure changes in water levels that contribute to the mass flux between a main channel and its floodplain. For example, measurements of water exchange over an entire year are available for only one of the ~8000 Amazon floodplain lakes [*Lesack and Melack*, 1995]. Thus, to estimate water mass balances during the passage of a flood wave across large, lowland floodplains it is typically assumed that the water surface is horizontal and equal to the changing level of water in the axial channel [e.g., *Richey et al.*, 1989a; *Bedient and Huber*, 1992]. Here we demonstrate using remote sensing that this assumption can greatly oversimplify the complex water movements on large floodplains.

[4] Modeling and hence predicting the hydrologic, ecologic, and societal consequences of floods is limited by the nearly complete lack of water height (h) measurements across floodplains. Computations of water surface elevation and flow directions are usually based on assumptions of one-dimensional downstream pressure gradients. Two-dimensional computations that allow for transverse gradients [*Bates and De Roo*, 2000] are difficult to validate with field measurements. *Alsdorf et al.* [2000, 2005] demonstrated the utility of interferometric radar for documenting coarse resolution patterns of water surface change during floodplain drainage. Here, we illustrate the feasibility of documenting and interpreting water-surface elevation changes and flow fields during inundation on complex floodplains with unprecedented precision.

2. Interferometric SAR Data

[5] Interferometric processing of SAR data has been used over the past decade to measure centimeter-scale topographic displacements resulting from earthquakes [*Massonnet et al.*, 1993], the movement of glaciers [*Goldstein et al.*, 1993], and the Earth's topography (Shuttle Radar Topography Mission digital elevation model, SRTM DEM [*Farr et al.*, 2007]). However, only recently has the interferometric SAR method demonstrated its potential for measuring water level fluctuations at a similar accuracy because the method works only with flooded vegetation [*Alsdorf et al.*, 2000, 2001a, 2001b; *Lu et al.*, 2005; *Kim et al.*, 2005]. Water is a specular reflector, such that large off-nadir imaging angles of SARs cause radar pulses to reflect away from the antennae. Flooded vegetation scatters some specularly reflected radar energy back to the antenna, thus enabling an interferometric measurement. We used SAR data from JERS-1 (Japanese Earth Resources Satellite) and typical

[1]School of Earth Sciences, Ohio State University, Columbus, Ohio, USA.
[2]School of Geographical Sciences, University of Bristol, Bristol, UK.
[3]Bren School of Environmental Science & Management, University of California, Santa Barbara, Santa Barbara, California, USA.
[4]Department of Geography, University of Exeter, Penryn, UK.

0094-8276/07/2007GL029447

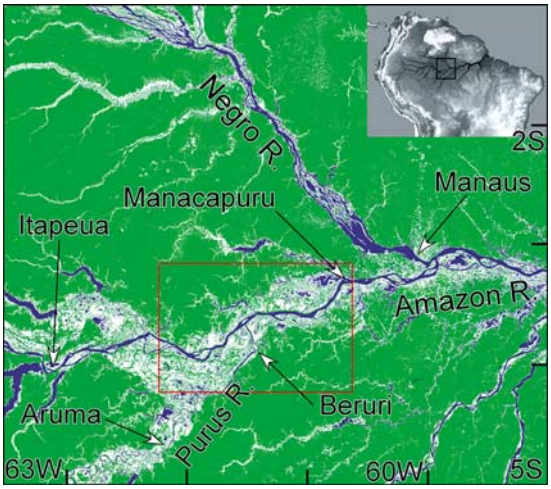

Figure 1. Study location. Overlay of two mosaics of JERS-1 L-band SAR images over the central Amazon Basin acquired during the low-water period of late 1995 and during peak stage in 1996 [*Rosenqvist et al.*, 2002]. White marks annually inundated areas; dark blues are always flooded; green is indicative of non-flooded areas [*Hess et al.*, 2003]. Red box locates Figures 2 and 4. Gauge locations are marked with arrows.

processing methods to construct multi-temporal interferograms showing water level changes over time. Because of the JERS-1 satellite repeat orbit, interferometric processing of the data produces a minimum Δt of 44 days with integer multiples thereafter. Unlike our previous work with SIR-C data (Spaceborne Imaging Radar C-Mission [*Alsdorf et al.*, 2000, 2001a]), the temporal phase coherence across the water surfaces is generally poor (i.e., less than 0.5). Fortunately, the interferometric JERS-1 phase values are spatially coherent because the water surfaces they measure extend across the ~50 km wide floodplain. Filtering methods enhance the phase but reduce the spatial resolution to about 200 m (Figure 2). This decreased temporal coherence results from the multi-day temporal baseline used in the JERS-1 interferograms, compared to the 24-hour baseline used with the SIR-C data [*Jung and Alsdorf*, 2006].

[6] Repeat pass interferometric SAR produces a relative mapping of Δh because the entire water surface is constantly moving up or down. In-situ measurements of Δh can be used to provide a datum but there are no gauges within the Amazon floodplain. Gauges are located only on the major river channels and are approximately referenced to the geoid yielding general trends in water level fluctuations with time. For example, from April 15 to July 12 of 1996 (the dates of the high water interferometric SAR data pair in Figure 2), gauged water levels at Itapeua rose 115 cm, at Beruri the rise was 146 cm, and at Manacapuru the increase was 152 cm. Thus $\partial h/\partial t$ increased downstream, agreeing with the interferometrically measured $\partial h/\partial t$ trends (Figure 2). Compared to Itapeua, Beruri water levels rose 31 cm higher (i.e., 146 – 115) and Manacapuru rose 37 cm higher. The interferometric measurements show a relative increase of 35 cm, agreeing with the gauge data. Similar agreement is found for the other 1993, 1996, and 1997 interferometric mappings.

[7] To demonstrate the complexity of water flow that is now evident in the $\partial h/\partial t$ maps of Figure 2, we used the Beruri gauge as a reference point and added one constant to

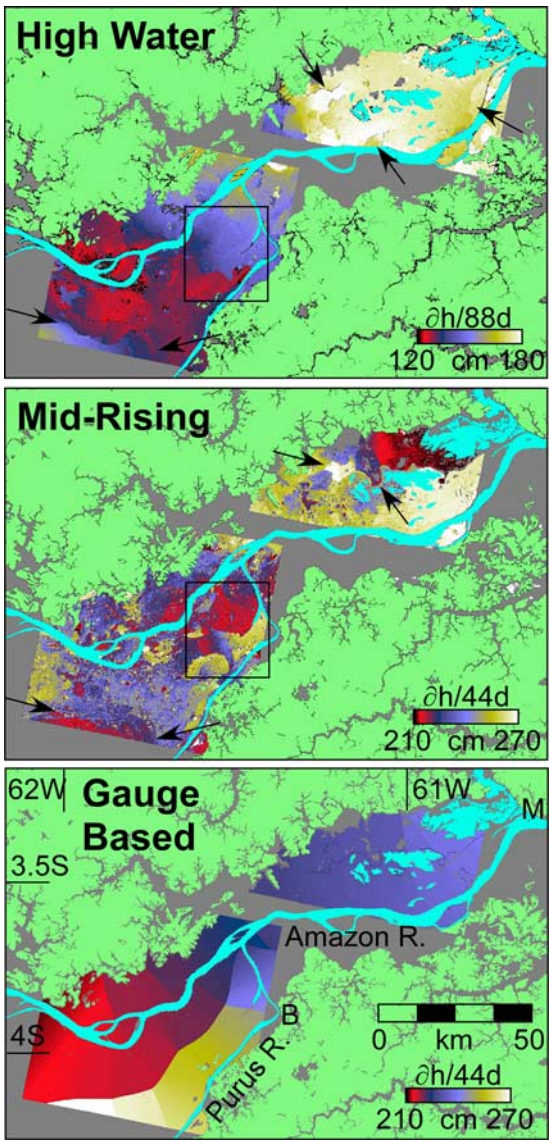

Figure 2. Measurements and estimates of $\partial h/\partial t$. Spatial patterns of temporal water level changes are measured from interferometric SAR between February 26 and April 11 (44 days in 1993, "Mid-Rising") and between April 15 and July 12 (88 days in 1996, "High Water"). Compare with $\partial h/\partial t$ surface estimated from stream gauge measurements using the same 1993 dates at Itapeua (west of figure, 4.1°S, 63.0°W), Beruri (marked with B), and Manacapuru (M). Gauge based estimate created by extrapolating perpendicularly the in-channel $\partial h/\partial t$ values, which are along-stream, linear interpolations from the three gauges (sharp change in $\partial h/\partial t$ located exactly mid-way between Amazon and Purus rivers is therefore a construct of the extrapolation). Light green colors indicate non-flooded, upland forests, grey marks floodplain areas for which no interferograms are available, and light blue are main rivers and permanent lakes which do not yield an interferometric measure of $\partial h/\partial t$. Arrows indicate locations of sharp changes in $\partial h/\partial t$. Box marks Figure 3.

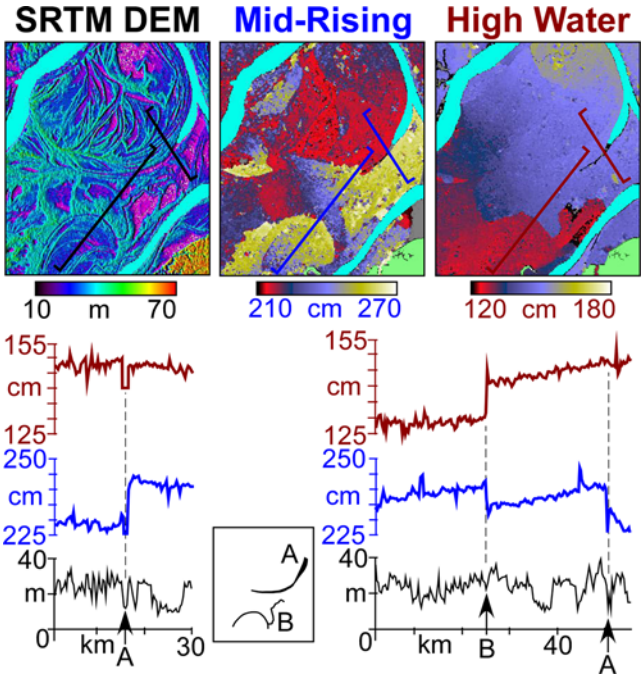

Figure 3. Detail of interferometric SAR measurements and topography. The Shuttle Radar Topography Mission digital elevation model (SRTM DEM) delineates the complex Amazon floodplain geomorphology (see Figure 2 for location). Sinuous channels are numerous. Blue and red lines locate profiles of $\partial h/\partial t$ at mid-rising and high water times, respectively, whereas black lines indicate floodplain topographic transects. Tic marks on plan view lines indicate view direction of profiles. Arrows A and B on plots note locations of two floodplain channels that coincide with sharp changes in $\partial h/\partial t$. Schematic in lower middle marks plan location of channels A and B.

an entire $\partial h/\partial t$ map so that interferometrically measured $\partial h/\partial t$ values within five kilometers equaled that of the gauge. Stream gauge data demonstrate the regularity of the annual Amazon flood wave [*Richey et al.*, 1989b; *Hamilton et al.*, 2002] with low water elevations occurring in October and high water in June, thus facilitating our usage of interferograms from three different years to represent general floodplain inundation.

3. Hydraulic Interpretation

[8] Prior to our interferometric SAR measurements, the best option for quantitative analysis of flows through large floodplains (spanning hundreds of kilometers) and the associated main channel, was to assume that floodplain water levels and changes were equivalent to those in the nearest axial river channel. The differences in $\partial h/\partial t$ between this assumed approach and the actual $\partial h/\partial t$ mid-rising measurements are striking (Figure 2). These differences clearly indicate that one-dimensional, point-based extrapolations from in-channel stream height measurements are inadequate to define flow across floodplains. Water flow velocities and directions within a floodplain can change with the passage of the flood wave, unlike river channels where waters are confined within banks and flow directed down the topographic slope. Such floodplain and wetland complexity has been inferred or measured by fluvial researchers in some field studies [e.g., *Filgueira-Rivera et al.*, 2007; *Hamilton and Lewis*, 1987; *Lewis et al.*, 2000], but this $\partial h/\partial t$ complexity has never been measured at the broad, synoptic scale we present.

[9] Temporal changes in water levels equate to spatial changes in discharge, i.e., $\partial h/\partial t \approx -\nabla \cdot Q$, where Q is discharge and h is the water surface elevation. Locations with positive $\partial h/\partial t$ values receive more water than is departing. In the absence of topographic barriers, flow is thus directed more toward large $\partial h/\partial t$ values. Three key interpretations of the interferometric mappings are based on this continuity approach.

[10] First, spatial trends in $\partial h/\partial t$ show abrupt changes that are spatially coincident with floodplain channels (Figure 3 and arrows in Figure 2). Based on the SRTM topography it is difficult to determine the magnitude of flow conveyance expected for a given channel because water surface gradient changes are subtle and boundary conditions are hard to specify in such a complex environment. For example, channels A and B (Figure 3) are not especially prominent when comparing their elevations, widths, or shapes to those of other floodplain channels. Yet, these two channels play a role in water flow across the floodplain as demonstrated by the spatially coincident sharp changes in $\partial h/\partial t$. During mid-rising conditions, water flow is directed mostly toward floodplain locations south of both channels. This water likely originates from the Purus River because the Purus flood wave arrives one month before that of the Amazon. At high water, flow directions switch and are directed to the north of channel B whereas the influence of channel A disappears. The Amazon flood peak creates backwater conditions on the Purus River [*Meade et al.*, 1991] such that the confluence is dominated by water originating from the Amazon.

[11] Second, during mid-rising conditions, the spatial patterns of water $\partial h/\partial t$ values are localized compared to high-water conditions where $\partial h/\partial t$ patterns extend more uniformly across the floodplain (Figure 2). At mid-rising time, the confined spatial patterns coupled with the spatial coincidence of floodplain channels with abrupt changes in $\partial h/\partial t$ likely indicates that water is flowing in confined, floodplain channel pathways and then dispersing only to the side where water levels were originally lower. At high water, however, the broad, smooth $\partial h/\partial t$ patterns indicate that water is flowing in a diffuse pattern across large portions of the floodplain.

[12] Third, flow across a floodplain is spatially complex for any given time and changes significantly during the passage of the flood wave. During mid-rising water, inundation appears first as a patchwork steered by the floodplain topography of scroll bars, levees, various types of floodplain channels, and depressions, whereas at peak stage, floodplain flow more closely parallels the Amazon River (Figure 4). Because these flow paths over the floodplain are not fixed in space and time, but vary with flood water elevations, they further build the wetland complexity by delivering sediments and nutrients from differing sources. For example, sediment concentrations from the river are higher during rising water [*Dunne et al.*, 1998], thus flow patterns at mid-rising times govern deposition. A given

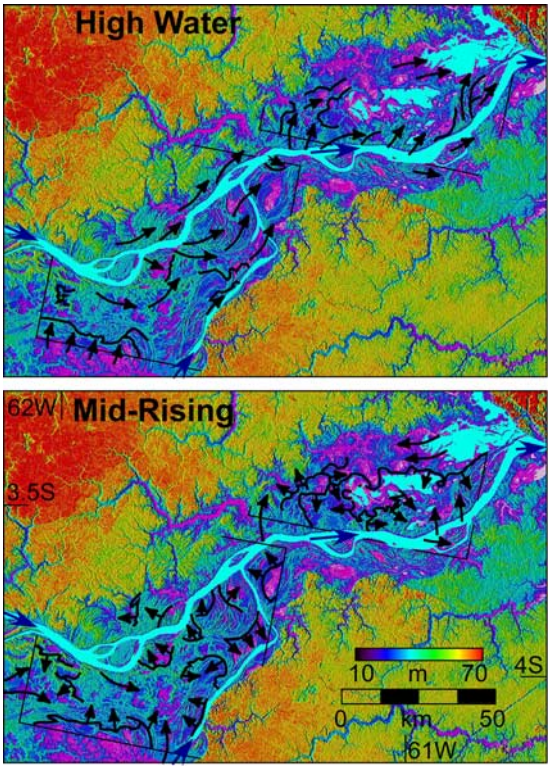

Figure 4. Water flow directions interpreted from measured $\partial h/\partial t$. Flow arrows are based on continuity with directions pointing toward areas of greater water accumulation, i.e., greater $\partial h/\partial t$ from Figure 2. Black lines mark channels that deliver water to the floodplain during mid-rising conditions or serve as leaky barriers to broad floodplain flows during high water. Mid-rising flow is multi-directional across the floodplain whereas high water flow is uni-directional, sub-parallel to the Amazon River.

location on the floodplain may first receive water from the Purus River and later receive water from the Amazon River. The complex flow paths result in adjacent floodplain areas having different mixtures of Purus and Amazon waters and hence different biogeochemistry. The first-order view of overbank flows [e.g., *Bates et al.*, 2006] supplying water to the floodplain along pathways sub-perpendicular to the main channel and of that water remaining on the floodplain before slowly decanting back to the main channel misses considerable complexity when based on standard topographic databases. Floodplains, flow paths, and residence times are dynamic, changing with the passage of the flood-wave. These flow paths and coupled $\partial h/\partial t$ values govern, in part, the mixing of nutrients, sediments, and organic matter that drive the ecology of a wetland.

4. Conclusions

[13] The implications of our work are:

[14] 1. This method reveals spatiotemporal patterns of water movement across floodplains with unprecedented detail, which will prove valuable for understanding how floodplains function and how they impact river hydrology and biogeochemistry. In the Amazon River system, floodplains and wetlands occupy ~20% of the watershed [*Melack and Forsberg*, 2001] and their influence on landscape-scale export of water and materials remains little understood.

[15] 2. The impact of floods on surrounding urban and agricultural areas can be better understood through such hydraulic mappings by providing a constrained, model-based prediction of flood water elevations [*Bates et al.*, 1997].

[16] 3. Design of large wetland restoration projects such as the Florida Everglades [e.g., *Schrope*, 2001] and the Mesopotamian Marshlands [*Richardson et al.*, 2005] could use spatially dense mappings of h, $\partial h/\partial t$, and $\partial h/\partial x$ in order to define the flow networks that might sustain the restored ecosystems.

[17] **Acknowledgments.** NASA's Programs in Terrestrial Hydrology, Large-Scale Biosphere Atmosphere experiment in Amazonia, and Solid Earth and Natural Hazards supported this research. JAXA supplied the JERS-1 data.

References

Alsdorf, D. E., J. M. Melack, T. Dunne, L. A. K. Mertes, L. L. Hess, and L. C. Smith (2000), Interferometric radar measurements of water level changes on the Amazon floodplain, *Nature*, *404*, 174–177.

Alsdorf, D. E., L. C. Smith, and J. M. Melack (2001a), Amazon floodplain water level changes measured with interferometric SIR-C radar, *IEEE Trans. Geosci. Remote Sens.*, *39*, 423–431.

Alsdorf, D., C. Birkett, T. Dunne, J. Melack, and L. Hess (2001b), Water level changes in a large Amazon lake measured with spaceborne radar interferometry and altimetry, *Geophys. Res. Lett.*, *28*, 2671–2674.

Alsdorf, D., T. Dunne, J. Melack, L. Smith, and L. Hess (2005), Diffusion modeling of recessional flow on central Amazonian floodplains, *Geophys. Res. Lett.*, *32*, L21405, doi:10.1029/2005GL024412.

Bates, P. D., and A. P. J. De Roo (2000), A simple raster-based model for floodplain inundation, *J. Hydrol.*, *236*, 54–77.

Bates, P. D., M. S. Horritt, C. N. Smith, and D. Mason (1997), Integrating remote sensing observations of flood hydrology and hydraulic modeling, *Hydrol. Processes*, *11*, 1777–1795.

Bates, P. D., M. D. Wilson, M. S. Horritt, D. Mason, N. Holden, and A. Currie (2006), Reach scale floodplain inundation dynamics observed using airborne synthetic aperture radar imagery: Data analysis and modeling, *J. Hydrol.*, *328*, 306–318.

Bedient, P. B., and W. C. Huber (1992), *Hydrology and Floodplain Analysis*, 2nd ed., 692 pp., Addison-Wesley, Boston, Mass.

Dunne, T., L. A. K. Mertes, R. H. Meade, J. E. Richey, and B. R. Forsberg (1998), Exchanges of sediment between the flood plain and channel of the Amazon River in Brazil, *Geol. Soc. Am. Bull.*, *110*, 450–467.

Farr, T., et al. (2007), The Shuttle Radar Topography Mission, *Rev. Geophys.*, doi:10.1029/2005RG000183, in press.

Filgueira-Rivera, M., N. D. Smith, and R. L. Slingerland (2007), Controls on natural levee development in the Columbia River British Columbia, Canada, *Sedimentology*, in press.

Goldstein, R. M., H. Engelhardt, B. Kamb, and R. M. Frolich (1993), Satellite radar interferometry for monitoring ice sheet motion: Application to an Antarctic ice stream, *Science*, *262*, 1525–1530.

Hamilton, S. K., and W. M. Lewis (1987), Causes of seasonality in the chemistry of a lake on the Orinoco River floodplain, Venezuela, *Limnol. Oceanogr.*, *32*(6), 1277–1290.

Hamilton, S. K., S. J. Sippel, and J. M. Melack (2002), Comparison of inundation patterns among major South American floodplains, *J. Geophys. Res.*, *107*(D20), 8038, doi:10.1029/2000JD000306.

Hess, L. L., J. M. Melack, E. M. Novo, C. Barbosa, and M. Gastil (2003), Dual-season mapping of wetland inundation and vegetation for the central Amazon basin, *Remote Sens. Environ.*, *87*, 404–428.

Jung, H.-C., and D. Alsdorf (2006), Repeat-pass multi-temporal interferometric SAR coherence variations with Amazon floodplain and lake habitats, *Eos Trans. AGU*, *87*(52), Fall Meet. Suppl., Abstract H23A-1459.

Kim, S. W., S. H. Hong, and J. S. Won (2005), An application of L-band synthetic aperture radar to tide height measurement, *IEEE Trans. Geosci. Remote Sens.*, *43*, 1472–1478.

Lesack, L. F. W., and J. M. Melack (1995), Flooding hydrology and mixture dynamics of lake water derived from multiple sources in an Amazon floodplain lake, *Water Resour. Res.*, *31*, 329–345.

Lewis, W. M., S. K. Hamilton, M. A. Lasi, M. Rodriguez, and J. F. Saunders (2000), Ecological determinism on the Orinoco floodplain, *BioScience*, *50*(8), 681–692.

Lu, Z., M. Crane, O.-I. Kwoun, C. Wells, C. Swarzenski, and R. Rykhus (2005), C-band radar observes water level change in swamp forests, *Eos Trans. AGU*, *86*(14), 141–144.

Massonnet, D., M. Rossi, C. Carmona, F. Adragna, G. Peltzer, K. Feigl, and T. Rabaute (1993), The displacement field of the Landers earthquake mapped by radar interferometry, *Nature*, *364*, 138–142.

Meade, R. H., J. M. Rayol, S. C. Da Conceicao, and J. R. G. Natividade (1991), Backwater effects in the Amazon River basin of Brazil, *Environ. Geol. Water Sci.*, *18*, 105–114.

Melack, J. M., and B. Forsberg (2001), Biogeochemistry of Amazon floodplain lakes and associated wetlands, in *Biogeochemistry of the Amazon Basin and its Role in a Changing World*, edited by M. E. McClain, R. L. Victoria, and J. E. Richey, pp. 235–276, Oxford Univ. Press, New York.

Richardson, C. J., P. Reiss, N. A. Hussain, A. J. Alwash, and D. J. Pool (2005), The restoration potential of the Mesopotamian marshes of Iraq, *Science*, *307*, 1307–1311.

Richey, J. E., L. A. K. Mertes, T. Dunne, R. L. Victoria, B. R. Forsberg, A. C. N. S. Tancredi, and E. Oliveira (1989a), Sources and routing of the Amazon River flood wave, *Global Biogeochem. Cycles*, *3*, 191–204.

Richey, J. E., C. Nobre, and C. Deser (1989b), Amazon river discharge and climate variability: 1903 to 1985, *Science*, *246*, 101–103.

Rosenqvist, A., M. Shimada, B. Chapman, L. Dutra, S. Saatchi, and O. Tanaka (2002), The Global Rain Forest Mapping project: Introduction from the guest editors, *Intl. J. Remote Sens.*, *23*(7), 1215.

Schrope, M. (2001), Save our swamp, *Nature*, *409*, 128–130.

D. Alsdorf, School of Earth Sciences, Ohio State University, Columbus, OH 43210-1308, USA. (alsdorf.1@osu.edu)

P. Bates, School of Geographical Sciences, University of Bristol, Bristol BS8 1SS, UK.

T. Dunne and J. Melack, Bren School of Environmental Science & Management, University of California, Santa Barbara, Santa Barbara, CA 93106-5131, USA.

M. Wilson, Department of Geography, University of Exeter, Penryn, TR10 9EZ, UK.